# Acousto–defect interaction in irradiated and non–irradiated silicon $n^+$–$p$–structure

O. Ya. Olikh,[1, a)] A. M. Gorb,[1] R. G. Chupryna,[1] and O. V. Pristay–Fenenkov[1]
*Faculty of Physics, Taras Shevchenko National University of Kyiv, Kyiv 01601, Ukraine*

(Dated: 21 November 2017)

The experimental investigation of ultrasound influence on the electrical characteristics of silicon $n^+$–$p$–structure has been carried out. The ultrasound induced effects in silicon structures, which have been exposed to reactor neutrons or $^{60}$Co gamma radiation, were studied too. It has been found out that the ultrasound loading of $n^+$–$p$–structure leads to reversible change of shunt resistance, carrier lifetime, and ideality factor. Acoustically induced alteration of the ideality factor and the space charge region lifetime depends on irradiation considerably. The models of coupled defect level recombination, Shockley–Read–Hall recombination, and dislocation–induced impedance were used to describe the obtained results. The observed phenomena can deal with the increase of distance between coupled defects as well as an extension of carrier capture coefficient of complex point defects and dislocations. The results show that divacancy and pair vacancy–interstitial oxygen are effectively modified by ultrasound in contrast to interstitial carbon–interstitial oxygen complex.

Keywords: acousto–defect interaction, silicon, irradiation

## I. INTRODUCTION

It is well known that ultrasound (US) can effectively interact with defects. As a defect engineering tool, US has the following advantages: (i) locality of action due to predominant absorption in the regions of lattice periodicity deviation; (ii) selectivity of influence, which depends on acoustic wave (AW) polarization and type; (iii) possibility to transform the defect system by applying resonance frequency; (iv) reversibility of effect of low intensity AW.

In piezoelectric semiconductors, the acousto–defect interaction (ADI) is mainly determined by electric field that accompanies the vibration wave propagation. However, ADI is also observed in such non–piezoelectric crystals as silicon, the basic material in microelectronic. Thus it was experimentally observed that US can cause atomic diffusion,[1,2] transformation of native and impurity defects,[3–7] modification of interior surface states,[8–10] appearance of new defects[11,12] in Si structures. Defects are known to determine most of semiconductor devices characteristics. In particular the ADI governs the variation of tunneling,[13,14] generation–recombination[15–17] and thermionic emission[18,19] currents in silicon barrier structures.

The change of population of impurity oscillator levels,[20] the displacement of impurity atoms with respect to their surroundings,[4,21,22] the decreasing of the diffusion activation energy,[23] the local temperature increase caused by point defect clusters[24] as well as the US absorption by dislocation[16,25,26] are believed to be the main mechanisms of elastic vibration–defect interaction in non–piezoelectric crystals. However to the best of our knowledge, there is no a comprehensive ADI theory for silicon suggested so far, the lack of experimental researches focused on acoustically induced (AI) effects being one of the main reasons.

The defects in silicon structures are not all acoustically active and can remain unmodified under the action of ultrasound. The ADI efficiency depends on defect type and structure.[8] Thus, the force acting on the point defect in the crystal under US loading (USL) of crystal is determined by the relaxation of defect volume[21,22]. The alterations of semiconductor defects are most widely produced by using the well–studied irradiation method. On the one hand, the high–power US treatment of irradiated silicon structures has been shown[27–30] to result in residual changes in structure properties. This effect deals with AI annealing of radiation defects (RDs). On the other hand, irradiation can be the reason of reversible AI phenomenon initiation,[31,32] which is caused by formation of acoustically active RDs. Unfortunately, there are but a few reports on acoustically driven phenomenon in irradiated silicon structures.

Our work presents the distinction between AI effects in silicon structures with different RDs. The intensity of the US applied was below the level of irreversible defect subsystem modification, which can deal with?? a new defect formation, RDs annealing or a long distance (a many interatomic distance) diffusion. As a result, the complete recovery of characteristics was observed after AW propagation had stopped.

The aim of our work is to investigate experimentally the AI electrical characteristic variation that takes place in non–irradiated and irradiated $n^+$–$p$–Si structures. For this purpose, the samples were irradiated by reactor neutrons and a $^{60}$Co–gamma source rays. It is supposed that $\gamma$–rays introduce predominantly $VO_i$ complex,[33–35] whereas neutrons mainly create vacancy clusters,[36,37] disordered regions,[38] and $C_iO_i$ complex.[35,39] Our work presents distinction of AI effects in silicon structures

a)Electronic mail: olikh@univ.kiev.ua

TABLE I. The sample irradiation parameters.

| Sample | Irradiation type | $D$ (rad) | $\Psi$ ($cm^{-2}$) | NIEL[a] (MeV $cm^2$/g) | $\Psi \times$NIEL (MeV/g) |
|---|---|---|---|---|---|
| iSC | non | 0 | 0 | — | 0 |
| nSC | neutron | $4.5{\cdot}10^3$ | $4{\cdot}10^{11}$ | $2.04{\cdot}10^{-3}$ | $8.2{\cdot}10^8$ |
| g6SC | $\gamma$–$^{60}$Co | $1{\cdot}10^6$ | $1.6{\cdot}10^{15}$ | $1.07{\cdot}10^{-7}$ | $1.7{\cdot}10^8$ |
| g7SC | $\gamma$–$^{60}$Co | $1{\cdot}10^7$ | $1.6{\cdot}10^{16}$ | $1.07{\cdot}10^{-7}$ | $1.7{\cdot}10^9$ |

[a] Ref. 44.

with different RDs. The intensity of applied US was *insufficient to* a new defect creation, a RDs annealing or a long distance (a many interatomic distance) diffusion. As a result, the *complete* recovery of characteristics was observed after AW propagation *had stopped*. *To describe the processes in space charge region (SCR) and in the diode base as well as to study shunt resistance, we used the models of coupled defect level recombination,*[40,41] *Shockley–Read–Hall (SRH) recombination and dislocation–induced impedance,*[42,43] *respectively. The observed AI phenomena are accounted for in terms of defect interaction with AW strain field.*[21,22] *Our research not only provides a better understanding of ADI* but could also facilitate the development of acoustically controlled devices or radiation sensors.

## II. EXPERIMENTAL AND CALCULATION DETAILS

*$n^+$-p–Si structure was fabricated from 2 inch (300 μm thick) p–type boron doped Czochralski silicon wafer with <111> orientation and resistivity of 10 Ω·cm.* The $n^+$ emitter with carrier concentration of about $10^{19}$ $cm^{-3}$ and thickness of 0.5 $\mu$m was formed by phosphorus implantation. *The* front and rear aluminium electrodes were deposited by screen printing before rapid annealing. *The samples used in the experiment were cut from the central part of the wafer and had the area of 2 $cm^2$. The* samples were irradiated by reactor neutrons or by $^{60}$Co $\gamma$–rays. *The* doses $D$, fluences $\Psi$, and sample labels are listed in Table I. *To determine D and Ψ correlation, the data from Refs. 44 and 45 were used.* The non–ionizing energy losses (NIEL) for neutron and $\gamma$–$^{60}$Co are *also* shown in Table I. Since *the* displacement damage effect is characterized by ($\Psi \cdot$NIEL), a similar damage was expected in *the* investigated samples *as well*. To avoid *the* impact of long–term annealing, which is typical to neutron damaged structure,[35,36] the irradiated samples *were* stored for 5 years at room temperature before *the measurements*.

The dark forward current–voltage ($I$–$V$) characteristics of the samples both with and without USL were measured over a temperature range of 290–340 K. The temperature was controlled by differential copper–constantan thermocouple. Some *of the obtained* curves are shown in Fig. 1.

The double–diode model of $n^+$–p structure $I$–$V$ characteristic is expressed in the following form:

$$I(V,T) = I_{SCR} + I_{base} + I_{sh}\,, \tag{1}$$

$$I_{SCR} = \frac{qAn_i d}{2\tau_g}\left\{\exp\left[\frac{q(V-IR_s)}{n_{\rm id}kT}\right]-1\right\}, \tag{2}$$

$$I_{base} = \frac{qAn_i^2}{p_p}\sqrt{\frac{\mu_n kT}{\tau_n}}\left\{\exp\left[\frac{q(V-IR_s)}{kT}\right]-1\right\}, \tag{3}$$

$$I_{sh} = (V-IR_s)/R_{sh}\,, \tag{4}$$

where $I_{SCR}$ describes the overall SCR recombination, $I_{base}$ is closely related to recombination in the quasi–neutral region, $I_{sh}$ is the shunt current, $A$ is the sample area, $n_i$ is the intrinsic carrier concentration, $\tau_g$ is the SCR carrier lifetime, $d$ is the SCR thickness:

$$d = \sqrt{\frac{2\varepsilon\varepsilon_0}{qp_p}\left[\frac{E_g}{q} - \frac{kT}{q}\ln\left(\frac{N_v N_c}{p_p n_n}\right) - \frac{2kT}{q} - V\right]}, \tag{5}$$

$\varepsilon$ is the permittivity (11.7 for Si), $p_p$ and $n_n$ are the majority carrier concentration in the $p$– and $n$–type regions, $E_g$ is the semiconductor band gap, $N_c$ and $N_v$ are the effective density of states in the conduction and valence bands; $n_{\rm id}$ is the ideality factor, $R_s$ and $R_{sh}$ are the series and shunt resistances, $\mu_n$ and $\tau_n$ are the electron (minority carrier) mobility and lifetime in the diode base.

We used Eqs. (1)–(5) to fit the experimental data *taking* $\tau_g$, $\tau_n$, $n_{\rm id}$, $R_{sh}$, and $R_s$ as the fittings parameters. *Also, we used* the known[46–48] temperature dependences of $n_i$, $E_g$, and $\mu_n$. *In the result, we obtained* extremely good fit to the experimental data — see Fig. 1. In particular, for all the samples the value of $R_s$ was found to be about 1 Ω. *The* broken lines in Fig. 1(a) *show* an example of *the* calculated contributions of $I_{SCR}$, $I_{base}$, and $I_{sh}$ to *full* current.

In *case of* USL , the transverse AWs with frequency of 4.2 MHz*, which* were exited *by using* piezoelectric transducer, were *applied to the samples at* the base side in the [111]–direction. The US intensities $W_{\rm US}$, amplitude of lattice deformation $\xi_{\rm US}$ and lattice atom displacement $u_{\rm US}$ are listed in Table II. It was reported previously[6,7,19] that the characteristic time of change in silicon structure parameters under the US action did not exceed $2 \cdot 10^3$ s. In order to wait the AI transitional period completion the following experimental procedure *was* used. *When USL started*, the sample *was first exposed to at room temperature for* 60 min and then the $I$–$V$ measurement and the sample heating were started. In order to avoid the effect of piezoelectric field on $I$–$V$ characteristics, the piezoelectric transducer *was* shielded.

Fig. 2 illustrates the reversibility of AI effects. The time interval between USL *initiation* and "during" measurement was *longer* than 60 min, the time interval between USL *termination* and "after" measurement was about 24 h. The data for nSC and g6SC are similar to those presented for iSC and g7SC.

The non-linear fittings were *performed* by using the differential evolution method.[49]

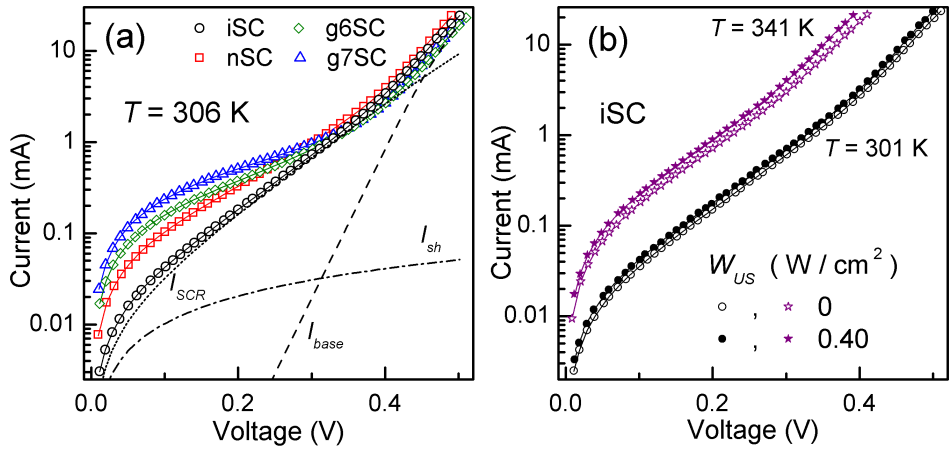


FIG. 1. Dark $I$–$V$ characteristics measured (a) at 306 K for non–irradiated (circles), neutron–irradiated (squares) and gamma–irradiated (diamonds and triangles) structures without USL; (b) at 301 K (circles) and 341 K (asterisks) with (filled marks, Ui–2) and without (open marks) USL for the iSC. The marks are the experimental results, the solid lines are the fitted curves using Eqs. (1)–(5). The dashed, dotted and dot–dashed lines in (a) represent the calculated base, SCR and shunt components of full (black solid line) iSC current.

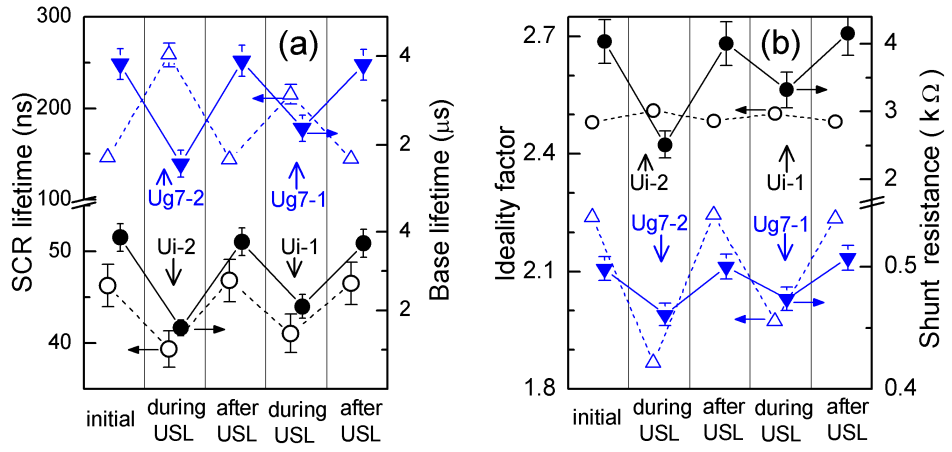


FIG. 2. SCR lifetime (a, left axis, open marks), base lifetime (a, right axis, filled marks), ideality factor (b, left axis, open marks) and shunt resistance (b, right axis, filled marks), obtained before, during and after USL at 330 K. Data for iSC (circles) and g7SC (triangles) are presented.

TABLE II. The ultrasound loading parameters.

| Sample | $W_{US}$ (W/cm$^2$) | $\xi_{US}$ ($10^{-6}$) | $u_{US}$ (nm) | USL label |
|---|---|---|---|---|
| iSC | 0.22 | 3.1 | 0.67 | Ui–1 |
| | 0.40 | 4.2 | 0.91 | Ui–2 |
| nSC | 0.24 | 3.2 | 0.70 | Un–1 |
| | 0.40 | 4.2 | 0.91 | Un–2 |
| g6SC | 0.38 | 4.1 | 0.89 | Ug6–2 |
| g7SC | 0.19 | 2.9 | 0.63 | Ug7–1 |
| | 0.37 | 4.0 | 0.87 | Ug7–2 |

## III. RESULTS AND DISCUSSION

### A. Space charge region

The parameters of $I$–$V$ characteristic *associated with* SCR phenomena are $n_{\rm id}$ and $\tau_g$. The temperature dependences of ideality factor and SCR carrier lifetime are shown in Fig. 3 and Fig. 4 respectively.

As shown *from* the Fig. 3, the ideality factor decreases with temperature increase and the dependence of $n_{\rm id}$ on $1/T$ is close to linear. Thus, dependence $n_{\rm id}(T)$ can be expressed as

$$n_{\rm id}(T) = n_{\rm id,\infty} + T_{\rm id}/T\,. \qquad (6)$$

The thermoactivated growth of SCR lifetime is observed over the explored temperature range — see Fig. 4. The

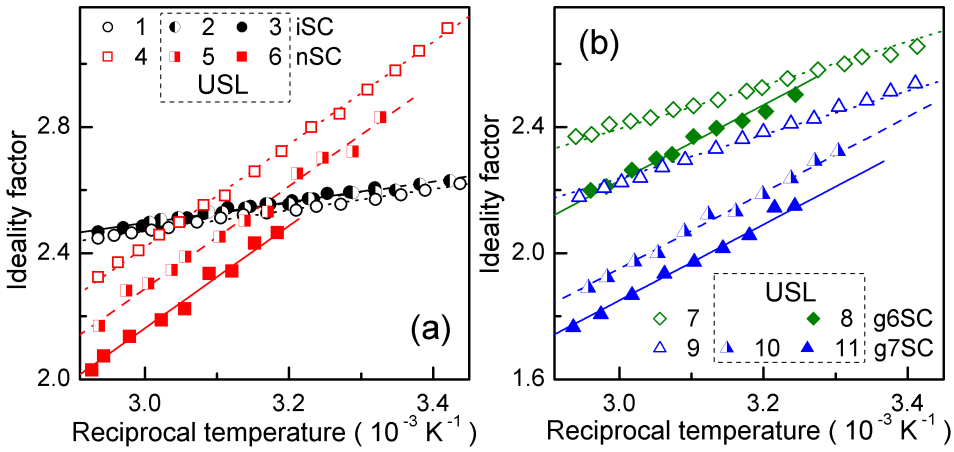


FIG. 3. Temperature dependences of ideality factor for non–irradiated (curves 1–3, circles), neutron–irradiated (4–6, squares) and $\gamma$–irradiated (7–11, diamonds and triangles) samples. The curves 1, 4, 7 and 9 (open marks) are obtained without USL, curves 2, 3, 5, 6, 8, 10, and 11 correspond to Ui–1, Ui–2, Un–1, Un–2, Ug6–2, Ug7–1, and Ug7–2 respectively. The marks are the experimental results, the lines are the fitted curves using Eq. (6).

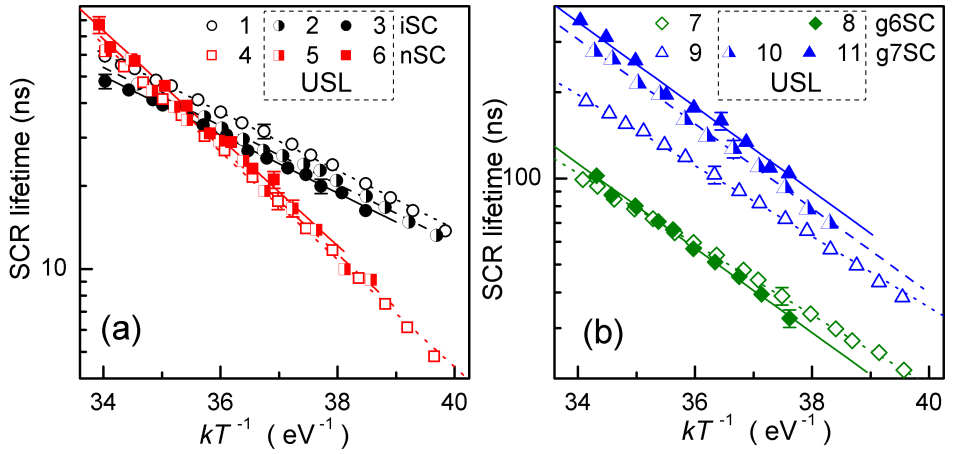


FIG. 4. Temperature dependences of SCR lifetime for non–irradiated (curves 1–3, circles), neutron–irradiated (4–6, squares) and $\gamma$–irradiated (7–11, diamonds and triangles) samples. The curves 1, 4, 7 and 9 (open marks) are obtained without USL, curves 2, 3, 5, 6, 8, 10, and 11 correspond to Ui–1, Ui–2, Un–1, Un–2, Ug6–2, Ug7–1, and Ug7–2 respectively. The marks are the experimental results, the lines are the fitted curves using Eq. (7).

temperature dependence of $\tau_g$ is well described by the equation

$$\tau_g(T) = \tau_{g0} \exp\left(-\frac{E_{\tau g}}{kT}\right) . \qquad (7)$$

The *values of* $T_{\rm id}$ and $E_{\tau g}$ *found* for both non–irradiated and irradiated samples under USL as well as without it are listed in Table III.

We *would like to* stress that

(i) irradiation leads to $T_{\rm id}$ and $E_{\tau g}$ changes, the g6SC's characteristic temperature of ideality factor and SCR lifetime characteristic energy are closely related to those of g7SC under similar conditions;

(ii) USL affects $n_{\rm id}$ and $\tau_g$ values; the absolute AI changes of ideality factor $\Delta n_{\rm id} = n_{\rm id,US} - n_{{\rm id},in}$ and the relative AI changes of SCR lifetime $\varepsilon_{\tau g} = (\tau_{g,\rm US} - \tau_{g,in})/\tau_{g,in}$ (where subscripts "US" and "*in*" *indicate* the values obtained at the same temperature with and without USL respectively) are listed in Table IV;

(iii) $\Delta n_{\rm id}$ and $\varepsilon_{\tau g}$ vary with $W_{\rm US}$ enhancement, whereas $T_{\rm id}$ and $E_{\tau g}$ values practically do not depend on US intensity;

(iv) USL leads to *the* increase *in* both $T_{\rm id}$ and $E_{\tau g}$ in $\gamma$–irradiated samples (see Fig. 3(b) and Fig. 4(b)), but this effect is not observed in non–irradiated and neutron–irradiated samples (see Fig. 3(a) and Fig. 4(a));

(v) $\Delta n_{\rm id}$ and $\varepsilon_{\tau g}$ have an opposite sign for non–irradiated and irradiated samples (for SCg6 not in whole temperature range);

(vi) ideality factor is varied by USL more effectively in irradiated samples.

For the purpose of *our analysis* it is important to dis-

TABLE III. Characteristics of temperature dependences of $n^+$–$p$–Si structure parameters.

| Sample | USL | $T_{\rm id}$ (K) | $E_{\tau g}$ (eV) | $R_{293,\rm A1}$ (kΩ) | $\sigma_{\rm dis}$ ($10^4$ K/Ω) |
|---|---|---|---|---|---|
| iSC | non | $330 \pm 30$ | $0.24 \pm 0.01$ | $27 \pm 3$ | $41 \pm 4$ |
| | Ui–1 | $310 \pm 30$ | $0.24 \pm 0.01$ | $27 \pm 3$ | $50 \pm 4$ |
| | Ui–2 | $360 \pm 30$ | $0.24 \pm 0.01$ | $26 \pm 3$ | $58 \pm 4$ |
| nSC | non | $1610 \pm 70$ | $0.45 \pm 0.02$ | $2.2 \pm 0.4$ | $65 \pm 7$ |
| | Un–1 | $1600 \pm 70$ | $0.44 \pm 0.02$ | $2.3 \pm 0.4$ | $95 \pm 10$ |
| | Un–2 | $1680 \pm 70$ | $0.44 \pm 0.02$ | $2.2 \pm 0.4$ | $130 \pm 10$ |
| g6SC | non | $610 \pm 40$ | $0.28 \pm 0.01$ | $0.7 \pm 0.1$ | $19 \pm 2$ |
| | Ug6–2 | $1080 \pm 50$ | $0.33 \pm 0.02$ | $0.8 \pm 0.1$ | $24 \pm 2$ |
| g7SC | non | $770 \pm 50$ | $0.29 \pm 0.01$ | $0.41 \pm 0.06$ | $26 \pm 3$ |
| | Ug7–1 | $1260 \pm 60$ | $0.34 \pm 0.02$ | $0.39 \pm 0.06$ | $45 \pm 4$ |
| | Ug7–2 | $1270 \pm 60$ | $0.35 \pm 0.02$ | $0.38 \pm 0.06$ | $55 \pm 4$ |

TABLE IV. Acoustically induced change of $n^+$-$p$–Si structure parameters (at 330 K).

| Sample | USL | $\Delta n_{\rm id}$ ($\pm 0.01$) | $\varepsilon_{\tau g}$ ($\pm 5\%$) | $\varepsilon_{\tau n}$ ($\pm 0.2$) | $\varepsilon_{\sigma \rm dis}$ ($\pm 10\%$) |
|---|---|---|---|---|---|
| iSC | Ui–1 | 0.02 | -14 | 0.7 | 20 |
| | Ui–2 | 0.03 | -17 | 1.4 | 40 |
| nSC | Un–1 | -0.13 | 5 | 1.5 | 50 |
| | Un–2 | -0.26 | 13 | 3.0 | 100 |
| g6SC | Ug6–2 | -0.15 | 2 | 2.3 | 30 |
| g7SC | Ug7–1 | -0.26 | 49 | 0.9 | 70 |
| | Ug7–2 | -0.36 | 70 | 1.9 | 110 |

cuss the recombination mechanism in SCR of the investigated samples. According to classical SRH theory, an ideality factor must be less than 2 and $\tau_g$ temperature dependence is expected[50,51] to be described by the relation $\tau_g \simeq 2\,\tau_n \sqrt{\sigma_n/\sigma_p}\cosh\left[(E_t - E_i)/kT\right]$ (where $\sigma_n$, $\sigma_p$, and $E_t$ are the electron and hole capture cross sections (CCSs) and the energy level of the recombination center, $E_i$ is the intrinsic energy level). In our case, $n_{\rm id}$ is lager than 2 and $\tau_g$ increases with temperature. Therefore, SRH theory *cannot be applied in our case.* Several attempts to *account for* large $n_{\rm id}$ value have been made *by using different* models.[52–55] *However,* all the observed features of SCR recombination (large ideality factor, independence on light intensity, dependence on temperature as well as *short carrier lifetime*) can be explained by the model of coupled defect level recombination (CDLR)[40,41] only. This mechanism provides a rapid direct charge transfer between defect levels. The phenomenon was *first* observed experimentally,[56,57] *after which* it was recruited to explain process in semiconductor diodes.[40,41,58]

According to CDLR model, recombination is the result of carrier exchange between two defect level and crystal bands. In particular, it is *supposed*[41] that the recombination rate is *dominant at the* sites where acceptor–like defect is coupled with donor-like defect. In simplified case, *when there is* no carrier exchange between the donor level $E_t^{\rm D}$ and the valence band, as well as between the acceptor level $E_t^{\rm A}$ and the conduction band, the recombination rate $R$ can be expressed[40] as

$$R = \frac{R_{12} - \sqrt{R_{12}^2 - 4\tau_n^{\rm D}\tau_p^{\rm A}(np - n_i^2)(1-\epsilon)}}{2\tau_n^{\rm D}\tau_p^{\rm A}(1-\epsilon)}\,, \qquad (8)$$

$$R_{12} = \frac{(n+n_{\rm D})(p+p_{\rm A})}{R_{\rm DA}} + \tau_n^{\rm D}(p+p_{\rm D}) + \tau_p^{\rm A}(n+n_{\rm A}), \qquad (9)$$

$$\tau_n^{\rm D} = (N_{\rm D}\,\sigma_n^{\rm D}\,\upsilon_{{\rm th},n})^{-1}, \quad \tau_p^{\rm A} = (N_{\rm A}\,\sigma_p^{\rm A}\,\upsilon_{{\rm th},p})^{-1}, \qquad (10)$$

where $R_{\rm DA}$ is the coupling parameter, $N_{\rm D}$ and $N_{\rm A}$ are the densities of donor and acceptor–like defects, $\sigma_n^{\rm D}$ and $\sigma_p^{\rm A}$ are electron CCS of donor and hole CCS of acceptor, $\upsilon_{{\rm th},n}$ and $\upsilon_{{\rm th},p}$ are the thermal electron and hole velocities, $n_{\rm D,A}$, $p_{\rm D,A}$, and $\epsilon$ depend on $E_t^{\rm D}$, $E_t^{\rm A}$, and level degeneracy factors. *Since* $\tau_g \propto R^{-1}$, the last three values are expected to provide a thermoactivated behavior of SCR lifetime. Unfortunately, the equation does not account for the functional relation between $I$–$V$ characteristic parameters and attributes of defects, taking part in CDLR.

According to Steingrube *et al.*[41], CCS for defect in a pair differs from that for *an* isolated defect and depends on the distance $r$ between donor and acceptor:

$$\sigma_{n,p}^{\rm D,A}(r) = C_{n,p}^{\rm D,A}\,r^2\,, \qquad (11)$$

where $C_n^{\rm D}$ and $C_p^{\rm A}$ are constant values. $R_{\rm DA}$ is proportional to the overlap integral of the defects wave functions too. If both defects are characterized by H–like radial–symmetric wave function, and equal Bohr radius $a_0$, the following expression can be used:[41]

$$R_{\rm DA}(r) \propto N_{\rm D}N_{\rm A}\left[1 + \frac{r}{a_0} + \frac{1}{3}\left(\frac{r}{a_0}\right)^2\right] e^{-r/a_0}\,. \qquad (12)$$

In our opinion, the observed reversible AI modifications of $n_{\rm id}$ and $\tau_g$ are induced by donor–acceptor distance alteration in samples under USL. In fact, according to data,[21,22] the force acting on the point defect during USL can be expressed as

$$F_d = \chi\,\Delta\Omega_d \frac{\partial \xi(z,t)}{\partial z}\,, \qquad (13)$$

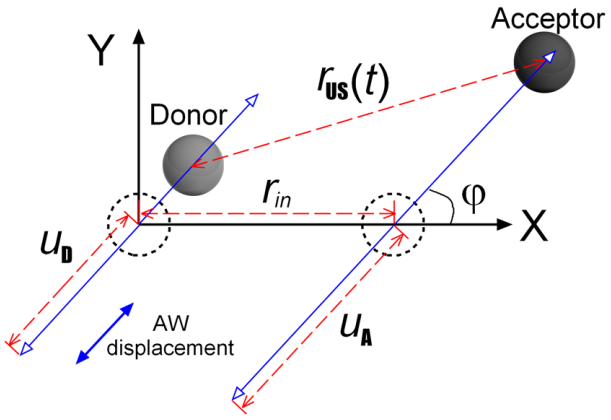


FIG. 5. Model of CDLR center behavior under US action.

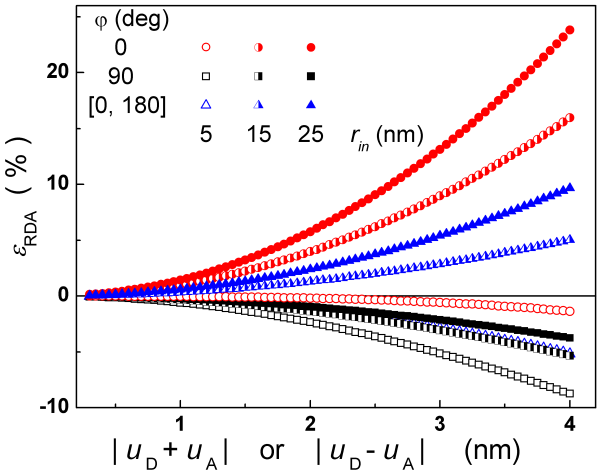


FIG. 6. Simulated dependencies of AI changes of coupling parameter on the vibration amplitudes. Axis $|u_D - u_A|$ corresponds to $\delta = 0°$ case, whereas axis $|u_D + u_A|$ corresponds to $\delta = 180°$ case. The parameters are set to $a_0 = 3.23$ nm, $r_{in} = 5$ nm (open marks), 15 nm (semi–filled marks), and 25 nm (filled marks), $\varphi = 0°$ (circles), 90° (squares). Triangles correspond to mean $\varepsilon_{RDA}$ value for $[0° \div 180°]$ $\varphi$ range.

where $\chi$ is the bulk elasticity modulus, $\Delta\Omega_d$ is the crystal volume change per defect, $\xi$ is the crystal lattice deformation, and AW propagates along $z$ axis, $\partial\xi(z,t)/\partial z \propto \xi_{US}$. $\Delta\Omega_d > 0$ for *the* interstitial atoms and substitutional impurities with ionic radius exceeding the ionic radius of matrix atoms, whereas for *the* vacancies and substitutional impurities *whose* ionic radius *is* smaller than that of matrix atoms $\Delta\Omega_d < 0$. Therefore, a point defect vibrates under USL, so oscillation amplitude and phase are determined by both the defect character and AW intensity.

The simplest model, which is shown in Fig. 5, gives the following qualitative conclusion. Initially, donor and acceptor are separated by the distance $r_{in}$, and axis X is drawn through *the* point defect initial positions. Under USL, *the* defects would vibrate with amplitudes $u_D$ and $u_A$. The vibration axis coincides with AW displacement direction and forms angle $\varphi$ with X–axis. *Depending on $\xi_{US}$, defect elastic strain ($\Delta\Omega_d^D$ and $\Delta\Omega_d^A$) and defect coupling the defect vibration amplitudes can have different values. The donor–acceptor distance in the sample under USL $r_{US}$, according to the model, depends on time $t$*:

$$r_{US}(t) = \left\{[r_{in} + u_A\cos(\omega_{US}t + \delta) - u_D\cos(\omega_{US}t)]^2\cos^2\varphi + [u_A\cos(\omega_{US}t + \delta) - u_D\cos(\omega_{US}t)]^2\sin^2\varphi\right\}^{0.5}, \quad (14)$$

where $\omega_{US}$ is the US cyclic frequency and $\delta$ is the phase shift between donor and acceptor vibration.

We use Eqs. (11)–(12) to estimate AI relative changes of CCS $\varepsilon_\sigma = [\sigma_{US} - \sigma(r_{in})]/\sigma(r_{in})$ and coupling parameters $\varepsilon_{RDA} = [R_{DA,US} - R_{DA}(r_{in})]/R_{DA}(r_{in})$, where $\sigma_{US}$ and $R_{DA,US}$ are averaged over the AW period $T_{US}$:

$$\sigma_{US} = \frac{1}{T_{US}}\int_0^{T_{US}}\sigma(r_{US}(t))dt\,,\; R_{DA,US} = \frac{1}{T_{US}}\int_0^{T_{US}}R_{DA}(r_{US}(t))dt\,.$$

In this estimation, the relaxation time in the CDLR subsystem is assumed to be considerably *shorter* than $T_{US}$, and we apply the previously used[41] value $a_0 = 3.23$ nm.

In addition, the chosen $u_D$ and $u_A$ values are commensurate with $u_{US}$. *However, it should be* taken into account, that the displacement of the point defect without covalent bond could exceed a matrix atom displacement. *Finally*, no US absorption by defect is assumed. In this simple case, $\delta$ *is equal* to 0° if $(\Delta\Omega_d^D \cdot \Delta\Omega_d^A) > 0$, or to 180° if $(\Delta\Omega_d^D \cdot \Delta\Omega_d^A) < 0$. In addition, $\varepsilon_{RDA}$ depends on $|u_D - u_A|$ ($\delta = 0°$ case) or $|u_D + u_A|$ ($\delta = 180°$ case). Moreover, these dependences are identical in both cases. The typical results of simulation of coupling parameter changes are shown in Fig. 6.

Relative changes of CCS depends on oscillation amplitudes with similar features and does not depend on $\varphi$:

$$\varepsilon_\sigma = (u_D \pm u_A)^2/2\,r_{in}^2 = K_{US}^{DA}W_{US}\,, \quad (15)$$

where"+" and "−" correspond to $\delta = 180°$ and $\delta = 0°$ respectively, $K_{US}^{DA}$ characterizes defect couple–ultrasound interaction and depends on properties defects as well as crystal matrix. Eq. (15) takes into account that $u_D, u_A \propto \xi_{US} \propto \sqrt{W_{US}}$.

It is worth keeping in mind that CDLR current flows locally in the locations of extended defects.[41,58] *At the same time, the* dislocations are often located perpendicularly to $p-n$ junction plane in the SCR region, and the investigated samples are not exception (see Section III C). If coupled defects and dislocations are close to each other, then the dislocations with edge component should affect the pair spatial orientation. Thus, the axis of donor–acceptor pair with $(\Delta\Omega_d^D \cdot \Delta\Omega_d^A > 0)$ should be predominantly parallel to dislocation line, whereas the axis of a pair of coupled defects with $(\Delta\Omega_d^D \cdot \Delta\Omega_d^A < 0)$ should make a right angle with *dislocation line*. As AW displacement is parallel to the $p-n$ junction plane, the cases of most

exciting interest are *the* following:
$\delta = 0°$, $\varphi = 90°$ ($\Delta\Omega_d^{\mathtt{D}} \cdot \Delta\Omega_d^{\mathtt{A}} > 0$ case);
$\delta = 180°$, $\varphi \in [0° \div 180°]$ ($\Delta\Omega_d^{\mathtt{D}} \cdot \Delta\Omega_d^{\mathtt{A}} < 0$ case).
In other words, all curves in Fig. 6 can be realized if defect volume relaxation of donor–like defect has the sign opposite to that of acceptor–like defect. *Moreover*, only squares *should* to be under consideration in case of $\Delta\Omega_d^{\mathtt{D}} \cdot \Delta\Omega_d^{\mathtt{A}} > 0$.

Taking into account the experimental results and the *estimation suggested by our model*:
(i) $E_{\tau g}$ and $T_{\mathrm{id}}$ are mainly determined by couple component energy levels. The alteration of $E_{\tau g}$ and $T_{\mathrm{id}}$ for nSC, g6SC, and g7SC in comparison with iSC testifies to the change of defect (donor, acceptor, or both) which take part in CDLR after irradiation. g6SC defect is coincident to g7SC defect and differs from neutron–irradiated sample defect.
(ii) USL causes donor–acceptor distance change and results in $\varepsilon_\sigma$ and $\varepsilon_{\mathtt{RDA}}$, which increase with $W_{\mathtt{US}}$.
(iii) Acoustically induced $E_{\tau g}$ (and $T_{\mathrm{id}}$) modification, which is observed in g6SC and g7SC only, testifies to the rebuilding of $\gamma$–induced RD, i.e., $\gamma$–induced RD is congurationally bistable (or metastable) and transforms from ground state under US action. Similar AI defect variations were also reported previously.[3,5,32,59]
(iv) $\varepsilon_\sigma$ sign is immutable — see Eq. (15), whereas $\varepsilon_{\mathtt{RDA}}$ sign can vary for the pair with opposite relaxation volume component (see Fig. 6). Therefore change of $\Delta n_{\mathrm{id}}$ and $\varepsilon_{\tau g}$ sign is the evidence of transformation from ($\Delta\Omega_d^{\mathtt{D}} \cdot \Delta\Omega_d^{\mathtt{A}} > 0$) to ($\Delta\Omega_d^{\mathtt{D}} \cdot \Delta\Omega_d^{\mathtt{A}} < 0$) after irradiation. The transformation is confirmed by *the enhanced efficiency of US action on defects* in irradiated samples. *In fact* in the case of ($\Delta\Omega_d^{\mathtt{D}} \cdot \Delta\Omega_d^{\mathtt{A}} < 0$) the US efficiency is determined by the sum of pair component displacements, whereas in the contrary case — by difference. In our opinion, both donor and acceptor are of interstitial–type defects in non–irradiated sample, and one of pair component is of vacancy–type defect in irradiated samples. The defect configuration are discussed below, in Section III D.

### B. Quasi–neutral region

Base lifetime describes the processes which occur in the quasi–neutral region of $p$-$n$–structure. Fig. 7 shows $\tau_n$ behaviour in the explored temperature range. *As expected,* minority carrier lifetime *increases as the temperature grows*, and at 320 K, $\tau_n$ values comprise $2 \div 5$ $\mu$s for different samples, which correspond to $80 \div 130$ $\mu$m range of diffusion lengths. In our opinion, the observed $\tau_n$ dispersion *is caused not by irradiation, but rather* deals with sample–ancestor wafer inhomogeneity, which *is often the case*.[60,61]

In fact the irradiation induced lifetime reduction is described by the Messenger-Spratt equation:[48]

$$\tau_n^{-1} = \tau_{n0}^{-1} + K_\tau \Psi \,, \qquad (16)$$

TABLE V. Measured and estimated base lifetime parameters.

| Sample | $\tau_{n,in}^{-1}$ (320 K) ($10^5$ s$^{-1}$) | $K_\tau$ (cm$^2$/s) | $K_\tau \times \Psi$ ($10^4$ s$^{-1}$) | $K_{\mathtt{US}}^{\mathtt{eff}}$ (cm$^2$/W) |
|---|---|---|---|---|
| iSC | 2.9 | — | — | 3.5 |
| nSC | 4.7 | $10^{-7}$(Ref. 33)<br>$2{\cdot}10^{-7}$(Ref. 62) | $4 \div 8$ | 7.1 |
| g6SC | 1.8 | $5{\cdot}10^{-12}$ | 0.8 | 6.0 |
| g7SC | 2.8 | (Refs. 33, 63) | 8 | 5.2 |

where $\tau_{n0}$ is the minority carrier lifetime in non–irradiated sample and $K_\tau$ is a lifetime damage–constants. The known $K_\tau$ values and estimated changes of reciprocal base lifetime $K_\tau \Psi$ are shown in the Table V. *As seen from the table,* the estimated value of radiation–induced $\tau_n^{-1}$ change comprise ($8 \div 17$), 4, and 29 % of its values measured for samples nSC, g6SC and g7SC, respectively, *so this* cannot explain the dispersion observed experimentally. *At the same time, the* calculated lifetime changes $K_\tau \Psi$ are in quite a good agreement with those expected from RDs production — see Section III D.

Base lifetime can be expressed as following:[64]

$$\tau_n^{-1} = \tau_{\mathtt{bb}}^{-1} + \tau_{\mathtt{CE\,Auger}}^{-1} + \tau_{\mathtt{SRH}}^{-1} \,, \qquad (17)$$

where $\tau_{\mathtt{bb}}$, $\tau_{\mathtt{CE\,Auger}}$, $\tau_{\mathtt{SRH}}$ are the lifetimes of band–to–band *recombination*, Coloumb–enhanced Auger *recombination*, and SRH recombination, respectively. *The* calculation shows that $\tau_{\mathtt{bb}}^{-1} = 14$ s$^{-1}$, $\tau_{\mathtt{CE\,Auger}}^{-1} = 6$ s$^{-1}$. Therefore band–to–band recombination and Auger recombination can be neglected. In case of low injection level and single recombination centre, SRH lifetime is described by Eq. (10). If there are several centers of recombination, the following equation should be applied

$$\tau_n^{-1} = \sum_i^{M_d} \tau_{n,i}^{-1} = \sum_i^{M_d} N_{d,i}, \sigma_{n,i}\, \upsilon_{\mathrm{th},n} \,, \qquad (18)$$

where $M_d$ is the total number of centers, $\tau_{n,i}$ characterizes lifetime due to recombination by $i$–th defect, $N_{d,i}$ and $\sigma_{n,i}$ are the concentration and electron CCS of $i$–th defect, respectively.

Fig. 7 shows that USL results in $\tau_n$ decrease. Relative AI changes of reciprocal base lifetime $\varepsilon_{\tau n} = (\tau_{n,in} - \tau_{n,\mathtt{US}})/\tau_{n,\mathtt{US}}$ are listed in Table IV. As AI changes are reversible, the lifetime alteration, in our opinion, deals with increase of $\sigma_n$ under US action. Following the empirical relation proposed by Ref. 65, we assume that Eq. (11) is *valid* for a complex point defect *as well*. *In this case, however,* $r$ is the distance which separates the components of a complex. According to the model suggested in Section III A, USL leads to $r$ variation and $\sigma_n$ change in line with Eq. (15). In case of CDLR, AI change of capture cross section of donor (or/and acceptor) is supplemental to the variation of both the coupling parameter and the couple distance, but only CCS change determines the AI variation of base lifetime.

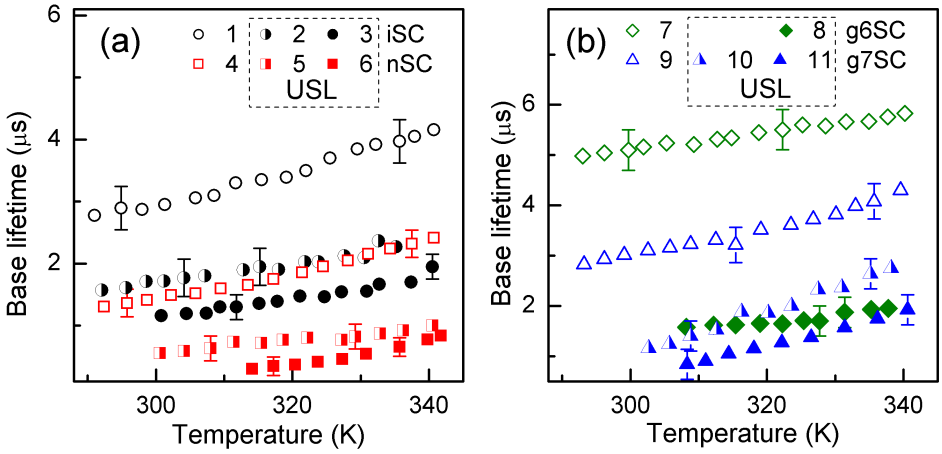


FIG. 7. Temperature dependences of base lifetime for non–irradiated (curves 1–3, circles), neutron–irradiated (4–6, squares) and $\gamma$–irradiated (7–11, diamonds and triangles) samples. The curves 1, 4, 7 and 9 (open marks) are obtained without USL, curves 2, 3, 5, 6, 8, 10, and 11 correspond to Ui–1, Ui–2, Un–1, Un–2, Ug6–2, Ug7–1, and Ug7–2 respectively.

*However*, not every defect effectively takes part in AID. If $M_d^{\mathtt{AA}}$ and $M_d^{\mathtt{nonAA}}$ are the total numbers of acoustically active (AA) and non–acoustically active (non–AA) centers, Eq (18) for $\tau_n^{-1}$ under USL and without it takes the following shape

$$\tau_{n,in}^{-1} = \sum_j^{M_d^{\mathtt{AA}}} N_{d,j}, \sigma_{n,j}^{in}\, \upsilon_{\mathrm{th},n} + \sum_l^{M_d^{\mathtt{nonAA}}} N_{d,l}, \sigma_{n,l}\, \upsilon_{\mathrm{th},n}\,,$$

$$\tau_{n,\mathtt{US}}^{-1} = \sum_j^{M_d^{\mathtt{AA}}} N_{d,j}, \sigma_{n,j}^{\mathtt{US}}\, \upsilon_{\mathrm{th},n} + \sum_l^{M_d^{\mathtt{nonAA}}} N_{d,l}, \sigma_{n,l}\, \upsilon_{\mathrm{th},n}\,.$$

*By* using Eq (15), $\varepsilon_{\tau n}$ *is transformed* as follows

$$\varepsilon_{\tau n} = K_{\mathtt{US}}^{\mathtt{eff}} W_{\mathtt{US}}\,, \tag{19}$$

where $K_{\mathtt{US}}^{\mathtt{eff}}$ characterizes ADI in the sample and depends on the concentration of both AA and non–AA centers

$$K_{\mathtt{US}}^{\mathtt{eff}} = \sum_j^{M_d^{\mathtt{AA}}} \frac{\tau_{n,in}}{\tau_{n,j,in}} K_{\mathtt{US,j}}\,, \tag{20}$$

$K_{\mathtt{US,j}}$ deals with $j$–th defect–ultrasound interaction.

The obtained dependences *of* $\varepsilon_{\tau n}$ vs $W_{\mathtt{US}}$ are shown in Fig. 8. *The* linearity of these dependences prove the correctness of our assumptions. The *obtained* $K_{\mathtt{US}}^{\mathtt{eff}}$ values are listed in Table V. The non–monotonic $K_{\mathtt{US}}^{\mathtt{eff}}$ alteration with $\gamma$ dose is discussed in Section III D.

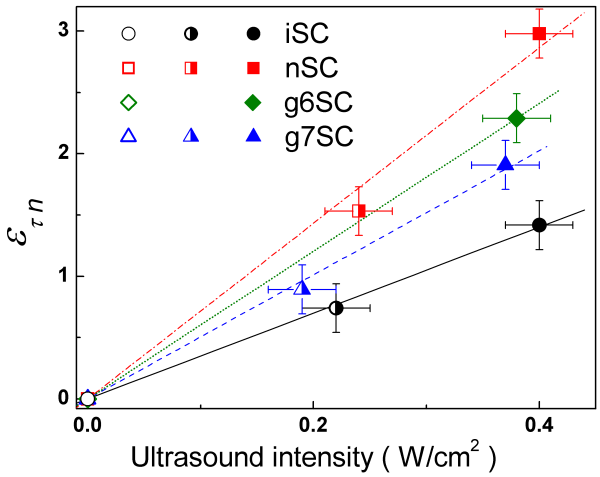


FIG. 8. Dependences of base lifetime relative change on US intensity for non–irradiated (circles), neutron–irradiated (squares), and $\gamma$–irradiated (triangles and diamonds) samples. Lines are the fitted curves using Eq. (19).

### C. Shunt resistance

Fig. 9 shows the shunt resistance over the explored temperature range. *As seen from the figure, the* irradiation results in $R_{sh}$ decrease. *Also,* the $R_{sh}$ temperature dependence changes after $\gamma$–irradiation. In particular the shunt resistance decreases with the temperature growth in iSC and nSC, whereas in g6SC and g7SC the increase of $R_{sh}$ vs $T$ i*s close to linear at the vicinity of* 293 K. *It should be noted* that $R_{sh}$ axis is logarithmic in Fig. 9(a) and linear in Fig. 9(b).

*The shunt resistance is known*[66] *to occur in p–n structure due to several non–mechanical reasons. It can be caused* by aluminum particles, macroscopic $Si_3N_4$ inclusions or inversion layers at precipitates. In the course of firing, Al particle *can* penetrate into the sample creating $p^+$–doped region around it, which compensates the emitter and remains in ohmic contact with the base. Inversion layers and $Si_3N_4$ inclusions occur mainly in multicrystalline silicon cells[66] and cannot cause shunt resistance in the investigated samples. *Dislocations, however,* which intersect the junction, are generally held responsible as

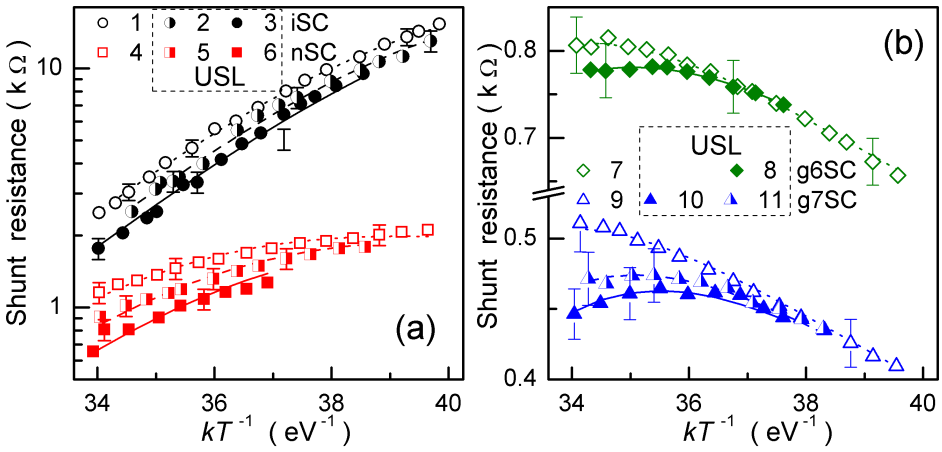


FIG. 9. Temperature dependences of shunt resistance for non–irradiated (curves 1–3, circles), neutron–irradiated (4–6, squares) and $\gamma$–irradiated (7–11, diamonds and triangles) samples. The curves 1, 4, 7 and 9 (open marks) are obtained without USL, curves 2, 3, 5, 6, 8, 10, and 11 correspond to Ui–1, Ui–2, Un–1, Un–2, Ug6–2, Ug7–1, and Ug7–2 respectively. The marks are the experimental results, the lines are the fitted curves using Eq. (21)-(23).

a possible source of ohmic current.[66–68] In our opinion, both aluminum particles and dislocations are present in the investigated structure, so the overall shunt resistance can be expressed as

$$R_{sh}^{-1} = R_{sh,\mathtt{Al}}^{-1} + R_{sh,\mathtt{dis}}^{-1}\,, \tag{21}$$

where $R_{sh,\mathtt{Al}}$ and $R_{sh,\mathtt{dis}}$ deal with aluminum particles and dislocations, respectively. The linear temperature dependence of metal particles $R_{sh,\mathtt{Al}}$ is suggested:

$$R_{sh,\mathtt{Al}} = R_{293,\mathtt{Al}}[1 + \alpha(T - 293)]\,, \tag{22}$$

where $R_{293,\mathtt{Al}}$ is the shunt resistance at 293 K and $\alpha$ is the resistance temperature coefficient.

According to the model of dislocation–induced impedance of photovoltaic detector suggested by Gopal and Gupta,[42,43] $R_{sh,\mathtt{dis}}$ can be given by:

$$R_{sh,\mathtt{dis}} = \frac{T}{\sigma_{\mathtt{dis}}}\left[\cosh\left(\frac{E_{\mathtt{dis}} - E_i}{kT}\right) + \cosh\left(\frac{U_s}{kT}\right)\right], \tag{23}$$

with

$$\sigma_{\mathtt{dis}} = \rho_{\mathtt{dis}} A q^2 A_{\mathtt{dis}} \sqrt{K_n K_p}\, N_{\mathtt{dis}}(n_p + p_p)/k\,, \tag{24}$$

where $E_{\mathtt{dis}}$ is the energy level which significantly contributes to the dislocation recombination current, $U_s$ is the potential at the surface of the dislocation core, $\rho_{\mathtt{dis}}$ and $A_{\mathtt{dis}}$ are the dislocation density and surface area, respectively, $K_n$ and $K_p$ are the probabilities for electrons and holes capture by the dislocation states, $N_{\mathtt{dis}}$ is the density of surface states at each dislocation. Eq. (23) *is true for* simplified case of $K_p = K_n$.

The resistance temperature coefficient was *estimated* from g7SC data. *The* obtained value $8.3 \cdot 10^{-3}$ K$^{-1}$ is not far from resistance temperature coefficient of bulk Al ($4.3 \cdot 10^{-3}$ K$^{-1}$). To fit the experimental data for $R_{sh}$ we used Eqs. (21)–(23). *As the fitting parameters,* $R_{293,\mathtt{Al}}$, $(E_{\mathtt{dis}} - E_i)$, $U_s$, and $\sigma_{\mathtt{dis}}$ were taken. It *has been found* that the experimental data are in good agreement with the fitting curves (see Fig. 9) for values $(E_{\mathtt{dis}} - E_i) = (0.46 \pm 0.02)$ eV and $U_s = (5 \pm 4) \times 10^{-8}$ eV, which were independent of irradiation and USL. The obtained value of $(E_{\mathtt{dis}} - E_i)$ corresponds to the carrier activation energy $0.10 \pm 0.02$ eV and is comparable *with* the activation energy of dislocation levels 0.08 eV, which was early reported[69–73] in Cz–Si:B too.[69–71]

Obtained values of $R_{293,\mathtt{Al}}$ and $\sigma_{\mathtt{dis}}$ are *given* in Table III. $R_{293,\mathtt{Al}}$ does not depend on USL and increases *as the* irradiation level. In our opinion, $R_{sh,\mathtt{dis}}$ is *smaller* than $R_{sh,\mathtt{Al}}$ in iSC. The irradiation *facilitates* to *the formation of vacancies as well as* Al diffusion out of the electrodes. As a *consequence*, the *number* of Al particles *grow*, $R_{sh,\mathtt{Al}}$ decreases and becomes the key factor *contributing in the* overall shunt resistance. Al *diffuses more effectively in the samples exposed to* $\gamma$–radiation due to a more uniform distribution of irradiation–induced single vacancies.

Dispersions of $\sigma_{\mathtt{dis}}$ and $\tau_n$ correlate on samples set. Hence $\sigma_{\mathtt{dis}}$ dispersion deals with wafer inhomogeneity too. USL *causes* $\sigma_{\mathtt{dis}}$ increase, relative AI changes $\varepsilon_{\sigma\mathtt{dis}} = (\sigma_{\mathtt{dis,US}} - \sigma_{\mathtt{dis},in})/\sigma_{\mathtt{dis},in}$ are shown in Table IV. In our opinion this is caused by an $A_{\mathtt{dis}}$ augmentation. Namely, the dislocation core atom displacement is normal to the current direction. As the result, the carriers are captured by dislocation levels from enlarged volume. Therefore, the effective surface area increases and $R_{sh,\mathtt{dis}}$ decreases *due to* US action.

### D. Defect type speculation

Lifetime killers in boron–doped Czochralski–grown Si are the boron–oxygen related (BO) defects,[74,75] iron–

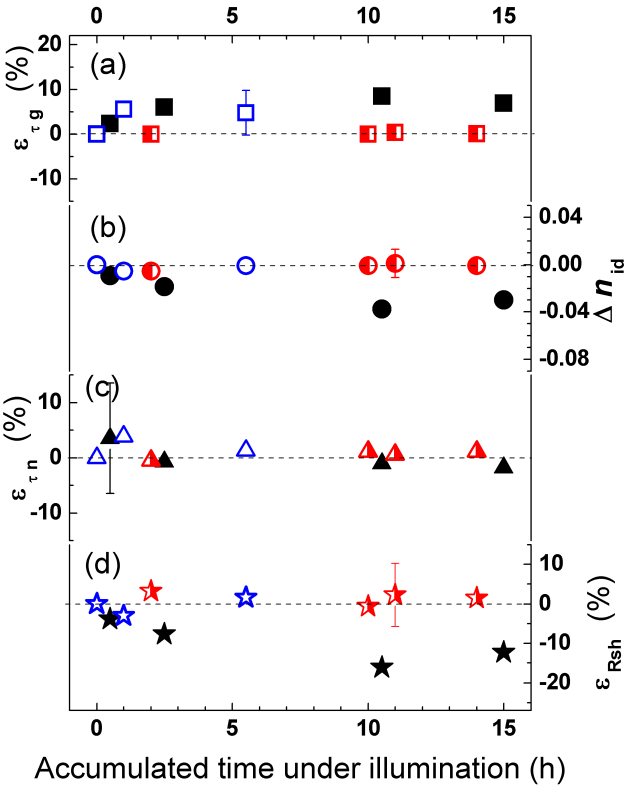


FIG. 10. Permanent changes of SCR lifetime (a, squares), ideality factor (b, circles), base lifetime (c, triangles), and shunt resistance (d, asterisks) versus accumulated illumination time. Sample iSC, $T$ = 295 K. Filled, semi–filled and open marks correspond to sample before annealing, after first 10 min 200 °C annealing, and after second 10 min 200 °C annealing, respectively.

boron pairs[64,76,77] (or another Fe–related trap in the $n^+p$–junctions[78,79]), and oxide precipitates.[60,61,64,80–82] The first two defects are sensitive to intensive illumination at room temperature. To determine the major recombination center of investigated samples the following experimental procedure has been used. The non-irradiated sample was light soaked under halogen lamp (2 Suns) illumination at approximately 305 K. The illumination varied from 1 h to 8 h. After illumination sample is stored in the dark at room temperature. To determine the kinetics of parameters the $I$–$V$ characteristics have been measured with interval 10–15 min at room temperature over a period 5 h after illumination stopping. To determine the permanent light–induced change the $I$–$V$ characteristics have been measured in 48 h after illumination. After accumulated time under illumination had run up to 15 h the iSC was annealed at 200 °C for 10 min in the dark and measurements were made at room temperature. After that, the illumination and measurements were repeated.

Intensive light is known[74,75] to lead to permanent transformation of BO defects and considerable decrease of minority–carrier lifetime (down to 10 % of initial value

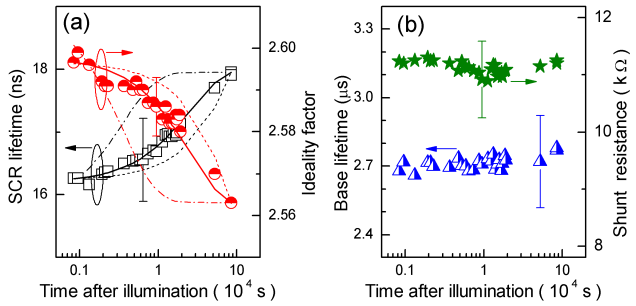


FIG. 11. SCR lifetime (a, squares, left axis), ideality factor (a, circles, right axis), base lifetime (b, triangles, left axis), and shunt resistance (b, asterisks, right axis) as a function of time since illumination stoping. Sample iSC, $T$ = 295 K. Lines are calculated by using Eqs.(25)–(26) and $E_{\mathrm{D,Fe}}$ = 0.63 eV (dash–dotted lines), 0.68 eV (solid lines), and 0.73 eV (dashed lines).

at long term illumination). Annealing at 200 °C for 10 min in the dark results in both BO defects state recovery and readiness of light–induced degradation. Fig. 10 show changes of structure parameters in comparison with those before illumination. One can see that illumination did not result in considerable permanent change of either of the $\tau_g$, $\tau_n$, $n_{\mathrm{id}}$ before as well as after annealing. Therefore BO influence on recombination can be neglected in both the SCR and the base.

On the other hand, the vast majority of impurity iron exists in iron–boron pairs. $\mathrm{Fe}_i\mathrm{B}_s$ can be readily dissociated under intense illumination to release interstitial iron. This gives a lifetime change. In dark $\mathrm{Fe}_i\mathrm{B}_s$ repairing takes place and $\mathrm{Fe}_i$ concentration decreases according to[64,83]

$$N_{Fe}(t) = (N_{Fe,0} - N_{Fe,eq}) \exp\left[-\frac{t}{\tau_{\mathtt{rep}}}\right] + N_{Fe,eq}\,, \quad (25)$$

where $N_{Fe,0}$ and $N_{Fe,eq}$ are the concentration after illumination immediately and equilibrium concentration which remains a long time after dissociation respectively, and the characteristic time of repairing $\tau_{\mathtt{rep}}$ depends on doping level

$$\tau_{\mathtt{rep}} = 770 \cdot p_p^{-2/3} \exp\left(\frac{E_{\mathtt{D,Fe}}}{kT}\right)\,, \quad (26)$$

$E_{\mathtt{D,Fe}}$ = 0.68 eV is the activation energy of $\mathrm{Fe}_i$ diffusion.

$n_{\mathrm{id}}$ increase (about 0.03) and $\tau_g$ decrease (about 10 %) immediately after illumination were observed — see Fig. 11(a). These changes vanished gradually. We supposed that the $\tau_g$ and $n_{\mathrm{id}}$ evolutions could be described by expressions, which like to Eq. (25). Then Eq. (26) was used to calculate characteristic time and fitting lines were plotted on Fig. 11(a). The fittings with $E_{\mathtt{D,Fe}}$ = 0.68 eV are in good agreement with experimental data. Hence iron–boron pairs take part in SCR recombination. On the other hand, electron and hole CCS of $\mathrm{Fe}_i$ are 1.7 and 0.04 times[64] as much as those of $\mathrm{Fe}_i\mathrm{B}_s$. A small (about 10 %) $\tau_g$ alteration, which is caused by light, is evidence

of supporting role of iron–boron pair in SCR recombination. Furthermore, since $\tau_n$ does not depend on illumination (see Fig. 11(b)), then $Fe_iB_s$ does not influence on base lifetime.

As a result, oxide precipitates are number one in SCR and base recombination. According to Murphy *et al.*[80,81], at least two independent oxide precipitate related defects exist. These defects have $\sigma_n/\sigma_p = 157$ and $\sigma_p/\sigma_n = 1200$ respectively.[81] So, they are suitable for CDLR. On the basis of mentioned above, we conclude that the defect, responsible for AI phenomena in nSC, is oxide precipitate mainly.

It is worth keeping doping level, oxygen concentration and irradiation dose in mind when RD type is foreseen. In our case (Czochralski, oxygen–rich, $\sim 7{\cdot}10^{17}$ cm$^{-3}$, $p$–Si with boron concentration $\sim 10^{15}$ cm$^{-3}$ and low dose) it is expected, that $C_iO_i$, vacancy clusters $V_n$ (divacancy $V_2$, trivacancy $V_3$, ...) and $VO_i$ are produced mainly by neutron irradiation[84–86] and $C_iO_i$ and $VO_i$ by $\gamma$–rays.[86–89] The RD concentration $N_{t,\mathtt{RD}}$ is proportionate to dose, the known introduction rate for neutron $\eta_n$ and gamma $\eta_\gamma$ irradiation in Cz–Si are shown in the Table VI. The expected values of $N_{t,\mathtt{RD}}$ for investigated samples are listed in the Table VI too.

Another defects, which can be created by irradiation in silicon, are $I_p$–center, bistable donor (BD), $B_iO_i$ and $C_iC_s$. But $I_p$–center and BD are characterized by small introduction rate. For example, expected[85,93] concentration of BD is only $(1\div2){\cdot}10^{10}$ cm$^{-3}$ in nSC and g7SC. The lack of $B_iO_i$ in investigated samples deals with low boron concentration[94]. Lastly, $C_iC_s$ creation is suppressed in oxygen–rich crystal.[84,87,88] Besides $C_iC_s$ is not recombination active center.[95]

The influence of RD on base lifetime could be estimated by Eq. (18) taking into account the fact, that $VO_i$ is not active recombination center in $p$–Si.[63,96–99] Estimated $\tau_{n,\mathtt{RD}}$ for $C_iO_i$, $V_2$, and $V_3$ are shown in Table VI. It shows that $\tau_n$ is effected mainly by $C_iO_i$ and vacancy clusters in $\gamma$– and neutron–irradiated samples, respectively. It should be noted, that nSC, g6SC, g7SC sums of $\tau_{n,\mathtt{RD}}$ are in quite good agreement with $(K_\tau \cdot \Psi)$ values.

Lets consider $K_{\mathtt{US}}^{\mathtt{eff}}$ assuming that $M_d^{\mathtt{AA}} = 1$, $M_d^{\mathtt{nonAA}} = 1$ in non–irradiated sample and US interaction with $C_iO_i$ and $V_n$ is described by $K_{\mathtt{US}}^{\mathtt{CO}}$ and $K_{\mathtt{US}}^{\mathtt{V}}$, respectively. Then Eq. (20) gives the following expression for $K_{\mathtt{US}}^{\mathtt{eff}}$ in nSC and irradiated samples:

$$K_{\mathtt{US}}^{\mathtt{eff}} = K_{\mathtt{US}}^{\mathtt{AA}}\,\tau_{n,in}/\tau_{n,in}^{\mathtt{AA}}\,,$$

$$K_{\mathtt{US}}^{\mathtt{eff}} = K_{\mathtt{US}}^{\mathtt{AA}}\tau_{n,in}/\tau_{n,in}^{\mathtt{AA}} + K_{\mathtt{US}}^{\mathtt{CO}}\tau_{n,in}/\tau_{n,\mathtt{RD}}^{\mathtt{CO}} + K_{\mathtt{US}}^{\mathtt{V}}\tau_{n,in}/\tau_{n,\mathtt{RD}}^{\mathtt{V}}\,.$$

$\tau_{n,in}^{\mathtt{AA}}$ is the base lifetime of the sample, where non-radiative AA defect with $K_{\mathtt{US}}^{\mathtt{AA}}$ is present only.

Two extreme cases are opportune for analysis. In the first one, non–AA defects are distributed uniformly across the wafer and AA defects define a distinction of $(\tau_{n,in}^{-1} - K_\tau \cdot \Psi)$ values in different samples. In the second one, a non–AA defect distribution is not uniform, whereas $\tau_{n,in}^{\mathtt{AA}}$ is identical for iSC, nSC, g6SC, and g7SC. However, in the first case (as well as in case of $M_d^{\mathtt{nonAA}} = 0$), experimental $K_{\mathtt{US}}^{\mathtt{eff}}$ values lead to unreal (negative) values of $K_{\mathtt{US,j}}$. In the second case, Eq. (20) and the data from the Tables V and VI, give the following array equations:

$$\begin{aligned}
\text{iSC}:\ & 3.5 = K_{\mathtt{US}}^{\mathtt{AA}} \cdot (\tau_{n,in}^{\mathtt{AA}})^{-1}\,/2.9\,,\\
\text{nSC}:\ & 7.1 = K_{\mathtt{US}}^{\mathtt{AA}} \cdot (\tau_{n,in}^{\mathtt{AA}})^{-1}\,/4.7 + 0.09\,K_{\mathtt{US}}^{\mathtt{V}} + 0.02\,K_{\mathtt{US}}^{\mathtt{CO}}\,,\\
\text{g6SC}:\ & 6.0 = K_{\mathtt{US}}^{\mathtt{AA}} \cdot (\tau_{n,in}^{\mathtt{AA}})^{-1}\,/1.8 + 0.01\,K_{\mathtt{US}}^{\mathtt{V}} + 0.05\,K_{\mathtt{US}}^{\mathtt{CO}}\,,\\
\text{g7SC}:\ & 5.2 = K_{\mathtt{US}}^{\mathtt{AA}} \cdot (\tau_{n,in}^{\mathtt{AA}})^{-1}\,/2.8 + 0.05\,K_{\mathtt{US}}^{\mathtt{V}} + 0.35\,K_{\mathtt{US}}^{\mathtt{CO}}\,,
\end{aligned}$$

where $(\tau_{n,in}^{\mathtt{AA}})^{-1}$ in $10^4$/ s. These equations are correct if $K_{\mathtt{US}}^{\mathtt{AA}}{\cdot}(\tau_{n,in}^{\mathtt{AA}})^{-1} = (10{\pm}3)$ cm$^2$/W, $K_{\mathtt{US}}^{\mathtt{V}} = (42{\pm}15)$ cm$^2$/W, $K_{\mathtt{US}}^{\mathtt{CO}} = 0$. Since $(\tau_{n,in}^{\mathtt{AA}})^{-1} < 1.83$, then $K_{\mathtt{US}}^{\mathtt{AA}} > 5$ cm$^2$/W. Thus observed change of the base lifetime is caused by AI modification of the same defect (most likely oxide precipitates) in both non–irradiated and $\gamma$–irradiated samples. This effect is added by AI divacancy alteration in neutron–irradiated samples. In other words, $C_iO_i$ is non–AA defect, whereas $V_2$ is AA defect.

As to SCR recombination, in our judgement, $\tau_g$ and $n_{\mathrm{id}}$ in non–irradiated sample are affected by modification of coupled oxide precipitate related defects under US action. As assumed above in Section III A, the AA radiation defects with $\Delta\Omega_d < 0$ take part in CDLR in irradiated samples. Divacancy is quite suitable explanation for AI influence on $\tau_g$ and $n_{\mathrm{id}}$ in nSC. But in $\gamma$–irradiated samples a bistable (or metastable) defect is expected. Few such defects with $\Delta\Omega_d < 0$ are known in Si, viz $VO_2$,[100] $V_3$,[91] and $VO_i$.[101] $VO_2$ appears after 300°C annealing of irradiated crystal, $V_3$ is not typical defect for $\gamma-{}^{60}$Co exposed silicon. On the other hand, $VO_i$ is largo manum produced and can take part in CDLR around $n^+$–$p$ interface in g6SC and g7SC. Metastable state, which is commonly observed at low temperature, is remarkable for the large oxygen–vacancy distance and more deep energy level.[101] The volume change of entire complex is negative, whereas for the complex component $\Delta\Omega_d(\mathrm{V}) < 0$ and $\Delta\Omega_d(\mathrm{O}_i) > 0$. Hence, under made assumption, $VO_i$ is favorable pair for AI alteration of distance between component. Thus $VO_i$ can be transformed into metastable configuration by USL and this effect results in both $T_{\mathrm{id}}$ and $E_{\tau g}$ change.

## IV. CONCLUSION

The experimental investigation of ultrasound influence on the $I$–$V$ characteristic of silicon $n^+$–$p$–structure has been carried out. The ultrasound induced effects in silicon structures, which have been exposed to reactor neutrons or $^{60}$Co gamma radiation, were studied too. The investigation revealed the acoustically driven reversible decrease of both the minority carrier lifetime in a structure base and the shunt resistance. The effect intensifies in irradiated structures. The analysis shows that the acoustically induced increase of carrier capture coefficient

TABLE VI. Cited and calculated defect parameters.

| Defect | $\sigma_n$ ($10^{-15}$ cm$^2$) | $\eta_n$ (cm$^{-1}$) Ref. 86 | $\eta_\gamma$ | $N_{t,\mathrm{RD}}(10^{11}$ cm$^{-3})$ nSC | g6SC | g7SC | $\tau_{n,\mathrm{RD}}^{-1}$ ($10^4$ s$^{-1}$) nSC | g6SC | g7SC |
|---|---|---|---|---|---|---|---|---|---|
| $C_iO_i$ | 0.7 (Ref. 87) | 1.38 | $6{\cdot}10^5$ rad$^{-1}$cm$^{-3}$ (Ref. 87) | 5.5 | 6 | 60 | $0.8 \div 1$ | $0.9 \div 1.1$ | $9 \div 11$ |
| | 0.9 (Ref. 88) | | $4{\cdot}10^{-4}$ cm$^{-1}$ (Ref. 88) | | | | | | |
| $V_2$ | 3 (Ref. 87) | 1.21 | $3{\cdot}10^4$ rad$^{-1}$cm$^{-3}$ (Ref. 87) | 4.8 | 0.3 | 3 | $2.2 \div 3.3$ | $0.1 \div 0.2$ | $1 \div 2$ |
| | 2 (Ref. 90) | | | | | | | | |
| $V_3$ | 2.4 (Ref. 91) | 0.37 | — | 1.5 | — | — | 0.7 | — | — |
| $VO_i$ | 2.4 (Ref. 89) | 0.52 | $7{\cdot}10^5$ rad$^{-1}$cm$^{-3}$ (Ref. 87) | 2 | $6 \div 7$ | $60 \div 70$ | | | |
| | 4 (Ref. 92) | | $4{\cdot}10^{-4}$ cm$^{-1}$ (Ref. 88) | | | | | | |

of point or extended defects is a reason of observed effects. It has been found out that the ultrasound loading leads to the reversible modification of SCR carrier lifetime and ideality factor. Changes are opposite in sign in non–irradiated and irradiated structures. The qualitative model of observed phenomenon, which is based on the increase of a distance between coupled defects or between defect complex components under ultrasound action, was considered. It has been shown that divacancy and pair vacancy–interstitial oxygen are effectively modified by ultrasound in neutron– and $\gamma$–exposed structures respectively. Interstitial carbon–interstitial oxygen complex does not practically take part in acousto–defect interaction. Thus, ultrasound can be an effective tool for controlling silicon structure characteristics.


[1] M. Jivanescu, A. Romanyuk, and A. Stesmans, J. Appl. Phys. **107**, 114307 (2010).
[2] A. Romanyuk, P. Oelhafen, R. Kurps, and V. Melnik, Appl. Phys. Lett. **90**, 013118 (2007).
[3] I. A. Buyanova, S. S. Ostapenko, M. K. Sheinkman, and M. Murrikov, Semicond. Sci. Technol. **9**, 158 (1994).
[4] O. Korotchenkov and H. Grimmliss, Phys. Rev. B **52**, 14598 (1995).
[5] O. Y. Olikh, Semiconductors **43**, 745 (2009).
[6] S. S. Ostapenko and R. E. Bell, Journal of Applied Physics **77**, 5458 (1995).
[7] I. Ostrovskii, O. Korotchenkov, O. Olikh, A. Podolyan, R. Chupryna, and M. Torres-Cisneros, J. Opt. A: Pure Appl. Opt. **3**, S82 (2001).
[8] D. Kropman, V. Seeman, S. Dolgov, and A. Medvids, phys. stat. sol. (c) **13**, 793 (2016).
[9] N. Zaveryukhina, E. Zaveryukhina, S. Vlasov, and B. Zaveryukhin, Technical Physics Letters **34**, 241 (2008).
[10] S. A. Mirsagatov, I. B. Sapaeva, and Z. Nazarov, Inorganic Materials **51**, 1 (2015).
[11] R. Savkina, A. Smirnov, T. Kryshtab, and A. Kryvko, Mater. Sci. Semicond. Process. **37**, 179 (2015).
[12] M. Virot, R. Pflieger, E. V. Skorb, J. Ravaux, T. Zemb, and H. Mohwald, J. Phys. Chem. C **119**, 15493 (2012).
[13] O. Y. Olikh, K. V. Voytenko, R. M. Burbelo, and J. M. Olikh, Journal of Semiconductors **37**, 122002 (2016).
[14] O. Olikh, Semiconductors **45**, 798 (2011).
[15] A. Davletova and S. Z. Karazhanov, Journal of Physics and Chemistry of Solids **70**, 989 (2009).
[16] A. Davletova and S. Z. Karazhanov, Journal of Physics D: Applied Physics **41**, 165107 (2008).
[17] V. Melnik, Y. Olikh, V. Popov, B. Romanyuk, Y. Goltvyanskii, and A. Evtukh, Materials Science & Engineering, B: Solid-State Materials for Advanced Technology **124–125**, 327 (2005).
[18] O. Y. Olikh, K. V. Voytenko, and R. M. Burbelo, Journal of Applied Physics **117**, 044505 (2015).
[19] O. Olikh, Ultrasonics **56**, 545 (2015).
[20] V. N. Pavlovich, phys. stat. sol. (b) **180**, 97 (1993).
[21] F. Mirzade, J. Appl. Phys. **110**, 064906 (2011).
[22] R. Peleshchak, O. Kuzyk, and O. Dan'kiv, Ukr. J. Phys. **61**, 741 (2016).
[23] V. D. Krevchik, R. A. Muminov, and A. Y. Yafasov, phys. stat. sol. (a) **63**, K159 (1981).
[24] F. Mirzade, J. Appl. Phys. **97**, 084911 (2005).
[25] I. Ostrovskii and O. Korotchenkov, Solid State Commun. **82**, 267 (1992).
[26] O. Olikh and K. Voytenko, Ultrasonics **66**, 1 (2016).
[27] N. Guseynov, Y. Olikh, and S. Askerov, Tech. Phys. Lett. **33**, 18 (2007).
[28] P. Parchinskii, S. Vlasov, and L. Ligai, Semiconductors **40**, 808 (2006).
[29] A. Gorb, O. Korotchenkov, O. Olikh, and A. Podolian, IEEE Trans. Nucl. Sci. **57**, 1632 (2010).
[30] A. O. Podolian, A. B. Nadtochiy, and O. A. Korotchenkov, Tech. Phys. Lett. **38**, 405 (2012).
[31] Y. Olikh, M. Tymochko, and A. Dolgolenko, Tech. Phys. Lett. **32**, 586 (2006).
[32] Y. Olikh and M. Tymochko, Tech. Phys. Lett. **37**, 37 (2011).
[33] H. Jafari and S. Feghhi, Nucl. Instrum. Methods Phys. Res., Sect. A **816**, 62 (2016).
[34] Y. P. Rao, K. Praveen, Y. R. Rani, A. Tripathi, and A. G. Prakash, Nucl. Instrum. Methods Phys. Res., Sect. B **316**, 205 (2013).
[35] M. Moll, H. Feick, E. Fretwurst, G. Lindström, and C. Schütze, Nucl. Instrum. Methods Phys. Res., Sect. A **388**, 335 (1997).
[36] J. Srour, C. Marshall, and P. Marshall, IEEE Trans. Nucl. Sci. **50**, 653 (2003).
[37] I. Pintilie, G. Lindstroem, A. Junkes, and E. Fretwurst, Nucl. Instrum. Methods Phys. Res., Sect. A **611**, 52 (2009).
[38] N. Arutyunov, N. Bennett, N. Wight, R. Krause-Rehberg, V. Emtsev, N. Abrosimov, and V. Kozlovski, phys. stat. sol. (b) **253**, 2175 (2016).
[39] C. A. Londos, G. Antonaras, and A. Chroneos, J. Appl. Phys. **114**, 193513 (2013).
[40] A. Schenka and U. Krumbein, Journal of Applied Physics **78**, 3185 (1995).
[41] S. Steingrube, O. Breitenstein, K. Ramspeck, S. Glunz, A. Schenk, and P. P. Altermatt, Journal of Applied Physics **110**, 014515 (2011).
[42] V. Gopal and S. Gupta, IEEE Trans. Electron Devices **50**, 1220 (2003).
[43] V. Gopal and S. Gupta, IEEE Trans. Electron Devices **51**, 1078 (2004).
[44] A. Akkerman, J. Barak, M. Chadwick, J. Levinson, M. Murat, and Y. Lifshitz, Radiat Phys Chem **62**, 301 (2001).
[45] D. Bräunig and F. Wulf, Radiat. Phys. Chem. **43**, 105 (1994).
[46] A. B. Sproul and M. A. Green, J. Appl. Phys. **73**, 1214 (1993).
[47] D. K. Schroder, *Semiconductor Material and Device Characterization*, 3rd ed. (John Wiley & Sons, New Jersey, 2006).

[48] A. McEvoy, T. Markvart, and L. Castaner, eds., *Solar Cells. Materials, Manufacture and Operation*, 2nd ed. (Academic Press, Oxford, 2013).
[49] K. Wang and M. Ye, Solid-State Electron. **53**, 234 (2009).
[50] D. Schroder, IEEE Trans. Electron Devices **29**, 1336 (1982).
[51] H. Aharoni, T. Ohmi, M. M. Oka, A. Nakada, and Y. Tamai, J. Appl. Phys. **81**, 1270 (1997).
[52] A. S. H. van der Heide, A. Schonecker, J. H. Bultman, and W. C. Sinke, Progress in Photovoltaics: Research and Applications **13**, 3 (2005).
[53] J. Beier and B. Voss, in *Proceedings of the 23rd IEEE Photovoltaic Specialists Conference* (1993) pp. 321–326, Louisville, KY, USA.
[54] J. M. Shah, Y.-L. Li, T. Gessmann, and E. F. Schubert, J. Appl. Phys. **94**, 2627 (2003).
[55] A. Kaminski, J. J. Marchand, H. E. Omari, A. Laugier, Q. N. Le, and D. Sarti, in *Proceedings of the 25th IEEE Photovoltaic Specialists Conference* (1996) pp. 573–576, Washington, DC, USA.
[56] W. M. Chen, B. Monemar, E. Janzén, and J. L. Lindström, Phys. Rev. Lett. **67**, 1914 (1991).
[57] A. M. Frens, M. T. Bennebroek, A. Zakrzewski, J. Schmidt, W. M. Chen, E. Janzén, J. L. Lindström, and B. Monemar, Phys. Rev. Lett. **72**, 2939 (1994).
[58] O. Breitenstein, J. Bauer, P. P. Altermatt, and K. Ramspeck, Solid State Phenomena **156–158**, 1 (2010).
[59] T. Wosinski, A. Makosa, and Z. Witczak, Semicond. Sci. Technol. **9**, 2047 (1994).
[60] L. Chen, X. Yu, P. Chen, P. Wang, X. Gu, J. Lu, and D. Yang, Sol. Energy Mater. Sol. Cells **95**, 3148 (2011).
[61] J. Schön, A. Youssef, S. Park, L. E. Mundt, T. Niewelt, S. Mack, K. Nakajima, K. Morishita, R. Murai, M. A. Jensen, T. Buonassisi, and M. C. Schubert, J. Appl. Phys. **120**, 105703 (2016).
[62] E. Gaubas, A. Uleckas, and J. Vaitkus, Nucl. Instrum. Methods Phys. Res., Sect. A **607**, 92 (2009).
[63] I. I. Kolkovskii, P. F. Lugakov, and V. V. Shusha, phys. stat. sol. (a) **83**, 299 (1984).
[64] J. D. Murphy, K. Bothe, M. Olmo, V. V. Voronkov, and R. J. Falster, J. Appl. Phys. **110**, 053713 (2011).
[65] D. G. Thomas, J. Hopfield, and W. M. Augistyniak, Phys. Rev. **140**, A202 (1965).
[66] O. Breitenstein, J. P. Rakotoniaina, M. H. Al Rifai, and M. Werner, Progress in Photovoltaics: Research and Applications **12**, 529 (2004).
[67] V. Gopal, J. Appl. Phys. **116**, 084502 (2014).
[68] I. Baker and C. Maxey, J. Electron. Mater. **30**, 682 (2001).
[69] A. Castaldini, D. Cavalcoli, A. Cavallini, and S. Pizzini, Phys. Rev. Lett. **95**, 076401 (2005).
[70] I. Isakova, A. Bondarenko, O. Vyvenko, V. Vdovin, E. Ubyivovk, and O. Kononchuk, Journal of Physics: Conference Series **281**, 012010 (2011).
[71] X. Yu, O. Vyvenko, M. Kittler, W. Seifert, T. Mtchedlidze, T. Arguirov, and M. Reiche, Semiconductors **41**, 458 (2007).
[72] V. Kveder, M. Kittler, and W. Schröter, Phys. Rev. B **63**, 115208 (2001).
[73] M. Trushin, O. Vyvenko, T. Mchedlidze, O. Kononchuk, and M. Kittler, Solid State Phenomena **156–158**, 283 (2010).
[74] J. Lindroos and H. Savin, Sol. Energy Mater. Sol. Cells **147**, 115 (2016).
[75] T. Niewelt, J. Schöon, W. Warta, S. W. Glunz, and M. C. Schubert, IEEE Journal of Photovoltaics **7**, 383 (2017).
[76] V. Vahanissi, A. Haarahiltunen, H. Talvitie, M. Yli-Koski, and H. Savin, Progress in Photovoltaics: Research and Applications **21**, 1127 (2012).
[77] J. Schmidt, Progress in Photovoltaics: Research and Applications **13**, 325 (2005).
[78] T. Mchedlidze and J. Weber, phys. stat. sol. (b) **251**, 1608 (2014).
[79] T. Mchedlidze, L. Scheffler, J. Weber, M. Herms, J. Neusel, V. Osinniy, C. Moller, and K. Lauer, J. Appl. Phys. **103**, 013901 (2013).
[80] J. Murphy, J. McGuire, K. Bothe, V. Voronkov, and R. Falster, Sol. Energy Mater. Sol. Cells **120**, 402 (2014).
[81] J. D. Murphy, K. Bothe, R. Krain, V. V. Voronkov, and R. J. Falster, J. Appl. Phys. **111**, 113709 (2012).
[82] M. Porrini and P. Tessariol, Materials Science and Engineering B **73**, 244 (2000).
[83] W. Wijaranakula, J. Etectrochem. Soc. **140**, 275 (1993).
[84] G. Lindström, M. Ahmed, S. Albergo, P. Allport, D. Anderson, L. Andricek, M. Angarano, V. Augelli, N. Bacchetta, P. Bartalini, R. Bates, U. Biggeri, G. Bilei, D. Bisello, D. Boemi, E. Borchi, T. Botila, T. Brodbeck, M. Bruzzi, T. Budzynski, P. Burger, F. Campabadal, G. Casse, E. Catacchini, A. Chilingarov, P. Ciampolini, V. Cindro, M. Costa, D. Creanza, P. Clauws, C. Da Via, G. Davies, W. De Boer, R. DellOrso, M. De Palma, B. Dezillie, V. Eremin, O. Evrard, G. Fallica, G. Fanouraki, H. Feick, E. Focardi, L. Fonseca, E. Fretwurst, J. Fuster, K. Gabathuler, M. Glaser, P. Grabiec, E. Grigorievt, G. Hall, M. Hanlond, F. Hauler, S. Heising, A. , Holmes-Siedle, R. Horisberger, G. Hughes, M. Huhtinen, I. Ilyashenko, A. Ivanov, B. Jones, L. Jungermann, A. Kaminsky, Z. Kohout, G. Kramberger, M. Kuhnke, S. Kwan, F. Lemeilleur, C. Leroy, M. Letheren, Z. Li, T. Ligonzo, V. Linhart, P. Litovchenko, D. Loukas, M. Lozano, Z. Luczynski, G. Lutz, G. MacEvoy, S. Manolopoulos, A. Markou, C. Martinez, A. Messineo, M. Mikuž, M. Moll, E. Nossarzewska, G. Ottaviani, V. Oshea, G. Parrini, D. Passeri, D. Petre, A. Pickford, I. Pintilie, L. Pintilie, S. Pospisil, R. Potenza, C. Raine, J. Rafi, P. Ratoff, H. Richter, P. Riedler, S. Roe, P. Roy, A. Ruzin, A. Ryazanov, A. Santocchia, L. Schiavulli, P. Sicho, I. Siotis, T. Sloan, W. Slysz, K. Smith, M. Solanky, B. Sopko, S. K., B. Sundby Avset, S. B., C. Tivarus, G. Tonelli, A. Tricomi, S. Tzamarias, G. Valvo, A. Vasilescu, A. Vayaki, E. Verbitskaya, P. Verdini, V. Vrba, S. Watts, E. Weber, M. Wegrzecki, I. Wegrzecka, P. Weilhammer, R. Wheadon, C. Wilburn, I. Wilhelm, R. Wunstorf, J. Wüstenfeld, J. Wyss, K. Zankel, P. Zabierowski, and D. Žontar, Nucl. Instrum. Methods Phys. Res., Sect. A **406**, 308 (2001).
[85] I. Pintilie, G. Lindstroem, A. Junkes, and E. Fretwurst, Nucl. Instrum. Methods Phys. Res., Sect. A **611**, 52 (2009).
[86] M. Moll, *Radiation damage in silicon particle detectors: Microscopic defects and macroscopic properties*, Ph.D. thesis, Universität Hamburg (1999).
[87] J. Stahl, E. Fretwurst, G. Lindström, and I. Pintilie, Nucl. Instrum. Methods Phys. Res., Sect. A **512**, 111 (2003).
[88] I. I. Kolkovskii and V. Lukyanitsa, Semiconductors **31**, 340 (1997).
[89] R. Siemieniec, W. Sudkamp, and J. Lutz, in *Proceedings of the Fourth IEEE International Caracas Conference on Devices, Circuits and Systems* (Oranjestad, Aruba, Netherlands, 2002) pp. D029–1–D029–6.
[90] S. D. Brotherton and P. Bradley, J. Appl. Phys. **53**, 5720 (1982).
[91] V. P. Markevich, A. R. Peaker, S. B. Lastovskii, L. I. Murin, J. Coutinho, V. J. B. Torres, P. R. Briddon, L. Dobaczewski, E. V. Monakhov, and B. G. Svensson, Phys. Rev. B **80**, 235207 (2009).
[92] H. Bleichner, P. Jonsson, N. Keskitalo, and E. Nordlander, J. Appl. Phys. **79**, 9142 (1996).
[93] E. Fretwurst, F. Hönniger, G. Kramberger, G. Lindström, I. Pintilie, and R. Röder, Nucl. Instrum. Methods Phys. Res., Sect. A **583**, 58 (2007).
[94] L. C. Kimerling, M. Asom, J. Benton, P. Drevinsky, and C. Caefer, Materials Science Forum **38–41**, 141 (1989).
[95] L. W. Song, X. D. Zhan, B. W. Benson, and G. D. Watkins, Phys. Rev. B **42**, 5765 (1990).
[96] J. L. Benton, S. Libertino, P. Kringhøj, D. J. Eaglesham, J. M. Poate, and S. Coffa, J. Appl. Phys. **82**, 120 (1997).
[97] S. Coffa, V. Privitera, F. Priolo, S. Libertino, and G. Mannino, J. Appl. Phys. **81**, 1639 (1997).

[98] N. Ganagona, B. Raeissi, L. Vines, E. V. Monakhov, and B. G. Svensson, phys. stat. sol. (c) **9**, 2009 (2012).
[99] L. Vines, E. V. Monakhov, A. Y. Kuznetsov, R. Kozłowski, P. Kaminski, and B. G. Svensson, Phys. Rev. B **78**, 085205 (2008).
[100] L. I. Murin, V. P. Markevich, I. F. Medvedeva, and L. Dobaczewski, Semiconductors **40**, 1282 (2006).
[101] B. N. Mukashev, K. A. Abdullin, and Y. V. Gorelkinskii, Physics–Uspekhi **43**, 139 (2000).